Available online at www.sciencedirect.com
SCIENCE DIRECT®
Journal of Power Sources 139 (2005) 152–164
JOURNAL OF POWER SOURCES
www.elsevier.com/locate/jpowsour

Direct hydrogen fuel cell systems for hybrid vehicles

Rajesh K. Ahluwalia*, X. Wang

Argonne National Laboratory, 9700 South Cass Avenue, Argonne, IL 60439, USA

Received 21 June 2004; accepted 20 July 2004
Available online 11 September 2004

Abstract

Hybridizing a fuel cell system with an energy storage system offers an opportunity to improve the fuel economy of the vehicle through regenerative braking and possibly to increase the specific power and decrease the cost of the combined energy conversion and storage systems. Even in a hybrid configuration it is advantageous to operate the fuel cell system in a load-following mode and use the power from the energy storage system when the fuel cell alone cannot meet the power demand. This paper discusses an approach for designing load-following fuel cell systems for hybrid vehicles and illustrates it by applying it to pressurized, direct hydrogen, polymer-electrolyte fuel cell (PEFC) systems for a mid-size family sedan. The vehicle level requirements relative to traction power, response time, start-up time and energy conversion efficiency are used to select the important parameters for the PEFC stack, air management system, heat rejection system and the water management system.

Keywords: Hydrogen fuel cell; Fuel cells for transportation; Thermal and water management; Air management; Fuel cells for hybrid vehicles; Cold start of fuel cell systems

1. Introduction

Automobile manufacturers are developing direct hydrogen, polymer-electrolyte fuel cell systems (PEFC) to provide traction power for passenger vehicles because of their promise of zero tailpipe emissions and improved fuel economy. Use of hydrogen for transportation also opens the window of opportunity for alternative infrastructure fuels including natural gas and biomass.

In contrast to the conventional internal combustion engines (ICE), fuel cell systems (FCS) have the characteristic that the efficiency does not degrade at part load and in fact can be much higher. This is particularly advantageous in transportation applications because the vehicles are mostly operated at part load conditions; the average demand on standard US drive cycles is less than 20% of the rated power of the engine. A recent study concluded that the fuel economy of hydrogen fuel cell vehicles can be 2.5–3 times the fuel economy of the conventional gasoline ICE vehicles [1].

Automobile manufacturers are developing gas-electric hybrids to overcome the limitations of the ICEs at part loads. Depending on the energy management strategy employed, hybridization allows the ICE to operate closer to the rated power while the energy storage device provides traction power at low loads. According to the different studies, hybridization has the potential to reduce the fuel consumption of gasoline ICE vehicles by 20–30% on standard US drive cycles [2,3].

Because the fuel cells are more efficient at part load than at rated power, the case for hybridizing a fuel cell vehicle is different. One motivation for hybridizing the FC vehicle is to improve its fuel economy by recovering a portion of the braking energy. Hybridization can also help if the energy storage device has higher specific power ($kW\,kg^{-1}$) and lower cost ($\$\,kW^{-1}$) than the FCS. Because of higher part-load efficiency, even in a hybrid configuration it appears advantageous to operate the FCS in a load-following mode and to use the power from the ESS when the FCS alone cannot meet the

* Corresponding author. Tel.: +1 630 252 5979; fax: +1 630 252 5287.
E-mail address: walia@anl.gov (R.K. Ahluwalia).

0378-7753/$ – see front matter © 2004 Published by Elsevier B.V.
doi:10.1016/j.jpowsour.2004.07.018

power demand. For hybrid vehicles, the fuel cell systems may couple best with high power, low energy storage devices such as supercapacitators.

The purpose of this paper is to present an approach for designing fuel cell systems for hybrid vehicles. We illustrate this approach by applying it to pressurized, direct hydrogen, polymer-electrolyte fuel cell systems in which the anode and cathode streams are externally humidified upstream of the PEFC stack and a pressurized condenser downstream of the stack recovers the process water. Alternate system configurations based, for example, on ambient pressure operation, internal stack humidification and enthalpy wheels for water recovery are possible but are not discussed in this paper.

2. System requirements

Fig. 1 shows the schematic of the pressurized direct hydrogen fuel cell systems analyzed in this study. At the rated power point, the PEFC stack operates at 2.5 atm and 80 °C to yield an overall system efficiency of 50% (based on lower heating value of hydrogen). Compressed hydrogen and air are humidified to 90% relative humidity at the stack temperature using process water and heat from the stack coolant. The system pressure is lower than 2.5 atm at part load and is determined by the operating map of the compressor–expander module. The nominal flow rate of cathode air is two times what is needed for complete oxidation of hydrogen (50% oxygen utilization). Process water is recovered from spent air in an inertial separator just downstream of the stack, in a condenser and in a demister at the turbine exhaust. The waste heat transferred to the coolant in the stack is either used for humidifying the anode and cathode streams or rejected in a radiator.

The thermal and water management system in Fig. 1 consists of two coolant circuits and a process water circuit. The high-temperature circuit delivers coolant (mixture of ethylene glycol and water) at 70–80 °C to the stack and rejects the stack waste heat in a dedicated air-cooled radiator. The high-temperature coolant also pre-heats the cathode and anode streams (to 70 °C at rated power) and provides the latent heats of humidification. The low-temperature circuit delivers coolant (mixture of ethylene glycol and water) at 55–70 °C to the shell-and-tube condenser and also cools the traction inverter motor (TIM) of the electric drive train. The condenser of the vehicle's air-conditioning (a/c) system can be cooled by means of the low-temperature coolant as well. The heat transferred to the low-temperature coolant in the FCS condenser, TIM and a/c condenser is rejected to the ambient in an air-cooled radiator. The two high-temperature and low-temperature circuits contain separate radiators but may share a coolant reservoir.

The process water circuit in Fig. 1 uses deionized (DI) water to humidify the anode and cathode streams. Under sustained driving conditions, the system is water neutral, i.e. the process water used in the humidifiers is recovered within the FCS. It may not be possible to completely recover the process water under all driving conditions, particularly during periods of rapid deceleration and at very low loads. However, the system can still be made water neutral by recovering excess water (produced in the stack) during favorable driving conditions (high loads and acceleration) to compensate for the net water consumed during unfavorable driving conditions.

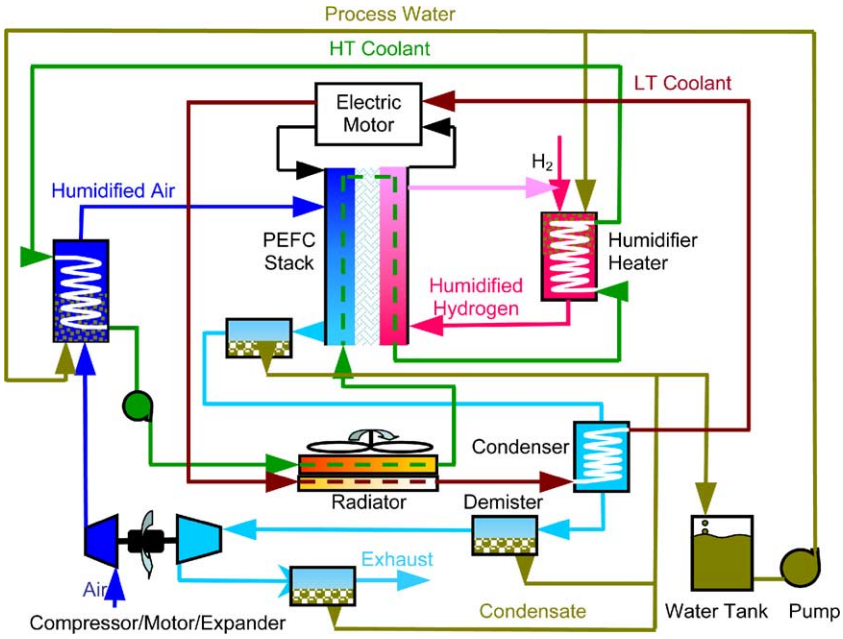

Fig. 1. Schematic diagram of a hydrogen-fueled, polymer-electrolyte fuel cell system for automotive applications.

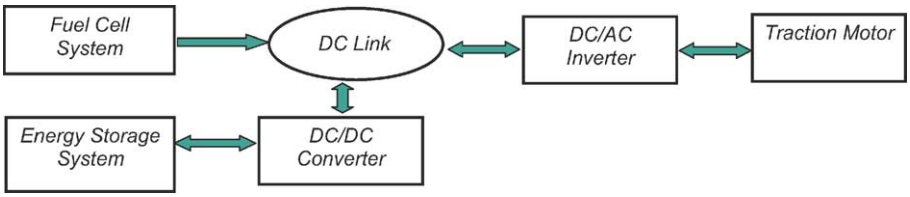

Fig. 2. Power train for a hybrid fuel cell vehicle.

Our interest is in a load-following FCS coupled to an energy storage system (ESS) operated in a charge-sustaining mode. In this type of a hybrid system (see Fig. 2), FCS generally provides the traction power under normal driving conditions with the ESS providing boost power under transient conditions. ESS also stores part of the energy that must otherwise be dissipated when the vehicle brakes. The manner in which the energy stored in ESS from regenerative braking is discharged and used for traction is determined by the vehicular energy management strategy. To be competitive with the conventional ICE propulsion system in terms of drivability and performance, the fuel cell system in this type of a hybrid vehicle must satisfy the following requirements:

(a) FCS alone must be capable of meeting the vehicle power demands under all sustained driving conditions. These include a specified top sustained speed, taken as 100 miles h^{-1} (mph) in this study, and ability to maintain the vehicle at 55 mph speed at 6.5% grade for 20 min.
(b) With the assistance of ESS, the FCS must have the response time to allow the vehicle to accelerate from 0 to 60 mph in a specified time, taken as 10 s in this study.
(c) FCS must have 1 s transient response time for 10–90% power.
(d) FCS must reach maximum power in 15 s for cold start from 20 °C ambient temperature.
(e) FCS must reach maximum power in 30 s for cold start from −20 °C ambient temperature.

The above requirements and the additional ones listed below can be used to size the stack system, air management system, heat rejection system, and the water management system. Summarized below is our approach for tailoring the fuel cell system to meet these requirements:

(a) We define the minimum power rating of the fuel cell system to be the higher of the power demand at 100 mph sustained speed and the power needed at 55 mph at 6.5% grade.
(b) We further require that the FCS be 50% efficient at the rated power point. This requirement determines the cell voltage at rated power.
(c) We require that the FCS be able to operate without overheating at ambient temperatures up to 42 °C. This requirement is met by sizing the heat rejection system for duty at the most stringent sustained driving condition on a 42 °C day.
(d) We size the water management system so that the FCS is water balanced for all sustained loads at 50% oxidant utilization and ambient temperatures up to 42 °C.
(e) We meet the 1 s transient time target by overloading the CEM electric motor for short time periods and, if needed, allowing the maximum oxidant utilization, generally limited to 50%, to rise to 60%.

We illustrate our approach by applying the methodology outlined above to determine the attributes of fuel cell systems for a typical mid-size family sedan with gross vehicle weight, frontal area, drag coefficient and coefficient of rolling friction listed in Table 1. The vehicle has a gross weight of 1900 kg that includes 1030 kg for the glider (body plus chassis), 136 kg for payload (cargo plus driver), 380 kg for the FCS, and 354 kg for the electric drive train. For this vehicle, Fig. 3 shows the power demand on the FCS as a function of vehicle speed and on 6.5% grade at 55 mph with 600 kg payload. In determining the power demand on the FCS, we have used a performance map for the traction inverter motor (TIM) that describes its efficiency as a function of the motor speed and torque. The TIM efficiency derived from the performance map is also presented in Fig. 3 as a function of vehicle speed and on 6.5% grade. The TIM efficiency peaks at 94% at 75 mph vehicle speed and drops to 84–85% as the speed is raised to 100 mph or lowered to 10 mph. In calculating power demand we have assumed peak efficiencies of 94% for the torque coupler and 97% for the final drive.

According to the results in Fig. 3, the traction power requirements for this vehicle are 65 kWe at 100 mph top speed and 62 kWe at 55 mph on 6.5% grade with 600 kg payload. We have also determined that the vehicle needs a peak power of about 120 kWe to be able to accelerate from 0 to 60 mph in 10 s. For this vehicle, the traction power at the top sustained speed (65 kWe) rather than at 6.5% grade defines the minimum power rating of the FCS so that systems of 65–120 kWe rated power are potential candidates. The 65 kWe FCS will need the largest ESS whereas the 120 kWe FCS can power the vehicle without an ESS.

Table 1
Vehicle specifications and traction power requirements

Vehicle specifications		Traction power requirements	
Gross vehicle weight	1900 kg	Z-60	120 kWe
Frontal area	2.0 m^2	Top speed (100 mph)	65 kWe
Drag coefficient	0.33	55 mph at 6.5% Grade	62 kWe
Coefficient of rolling friction	0.009		

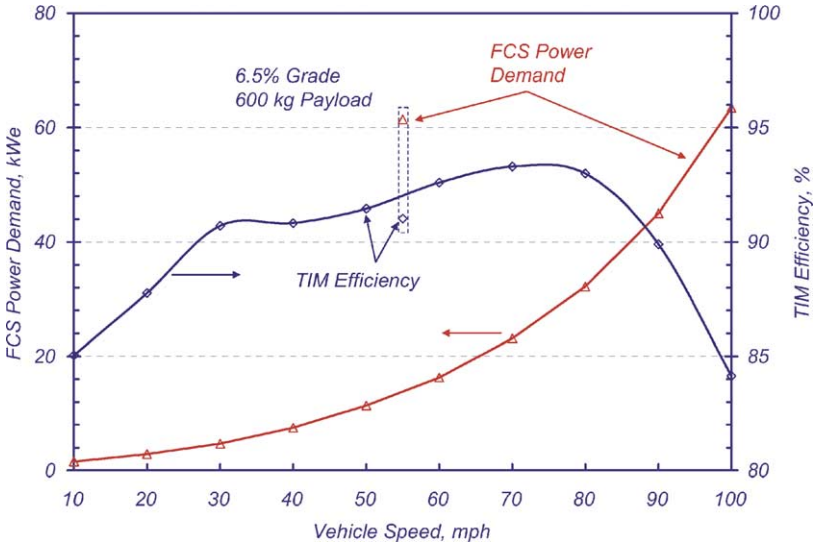

Fig. 3. FCS power demand vs. vehicle speed.

3. Fuel cell systems for hybrid vehicles

Table 2 summarizes the characteristics of four fuel cell systems analyzed using GCtool [4], a systems design and analysis software package developed at Argonne National Laboratory. These systems differ in power rating but otherwise have identical layout as configured in Fig. 1. We have also analyzed systems without an expander but these are mentioned only in passing. In this section, we discuss the characteristics of the four major components comprising the FCS: PEFC stack, air management system, heat rejection system, and the water recovery system. The overall performance of the fuel cell systems is discussed in the next section.

3.1. PEFC stack

The polarization curves used in this study are derived from a correlation of cell voltage as a function of current density, stack temperature and oxygen partial pressure. The experimental data underlying the correlation may be somewhat dated but bears proper trend with respect to the dependent variables. To be consistent with the recent announcements on the performance of GM2001 stack [5] and Ballard stack [6], PEFC system weights and volumes were estimated by using the published values of stack power density and specific power and adjusting them for the design-point cell voltage. We then renormalized the current density to match the assumed power density at the design point. Also, we do not have experimental data at freezing temperatures and the −20 °C stack data discussed below is merely extrapolation of the polarization curve obtained at room temperature.

Fig. 4 shows the behavior of the stack for the 100 kWe FCS at 50% oxidant utilization with the system pressure varying with air flow rate. At the design point, 80 °C stack temperature and 20 °C ambient temperature, the stack is sized to generate 110 kWe at 690 mV. The stack can actually generate more than the rated power, albeit at lower cell voltage. It can generate 125 kWe at 670 mV if the air management system is oversized to deliver air at 120% of the rated flow or the oxygen utilization is allowed to exceed 50%.

At 20 °C stack/ambient temperature, the cell voltage at rated flow (same current density as at the rated power point

Table 2
Fuel cell systems for the mid-size family sedan

	65 kWe	80 kWe	100 kWe	120 kWe
FCS efficiency				
At rated power (%)	50.0	50.0	50.0	50.0
At 25% of rated power (%)	59.6	59.6	59.6	59.6
At 65 kWe (%)	50.0	54.1	56.0	57.0
At 15 kWe (%)	59.7	60.0	60.1	60.4
Specific power (including H_2 storage) ($W\,kg^{-1}$)	230	260	290	315
Transient response (10–90% power) (s)	1.0	1.0	1.0	1.0
Cold start-up time (to maximum power)				
At −20 °C ambient temperature (s)	34.4	34.2	34.1	33.9
At 20 °C ambient temperature (s)	19.2	19.2	19.3	19.2

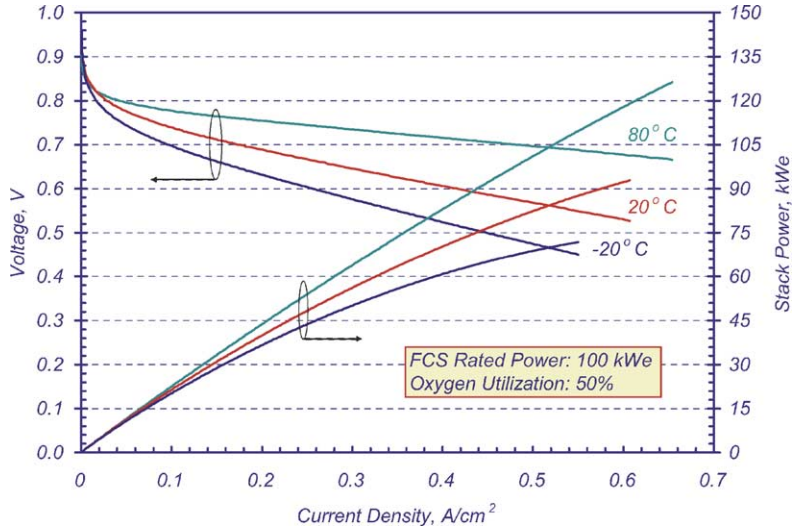

Fig. 4. Stack polarization curves and power for 100 kWe FCS.

at 80 °C) decreases to 550 mV and the stack power is derated by 20%. The maximum power that the stack can generate at 20 °C (93 kWe at 527 mV cell voltage) is actually limited by the amount of cathode air that can be delivered by the air management system.

At −20 °C ambient/0 °C stack temperature, the power that the stack can generate at rated flow is about 35% lower than at 80 °C stack temperature and the cell voltage further decreases to 450 mV. This is also the maximum power that the stack can generate at −20 °C since we limit the minimum cell voltage to 450 mV in our simulations. The allowable minimum cell voltage depends on the power electronics and can be lowered by placing a dc/dc converter between the PEFC stack and the traction inverter motor but the overall system efficiency will suffer.

3.2. Air management system

Simulation results presented in this study are based on the projected performance shown in Fig. 5 for a matched, single stage, turbo compressor–expander module (CEM) being developed at Honeywell [7]. The module is equipped with a high-speed ac induction motor and a motor controller that also includes a dc/ac inverter so that the module can be directly run by the dc power generated at the PEFC stack. Over the operating range, the motor has an average efficiency of about 91% and the motor-controller an average efficiency of about 92%. At the design point, the compressor delivers air at 2.5 atm and the compressor and expander have isentropic efficiencies of about 80% and 78%, respectively. The compressor discharge pressure as well as compressor and

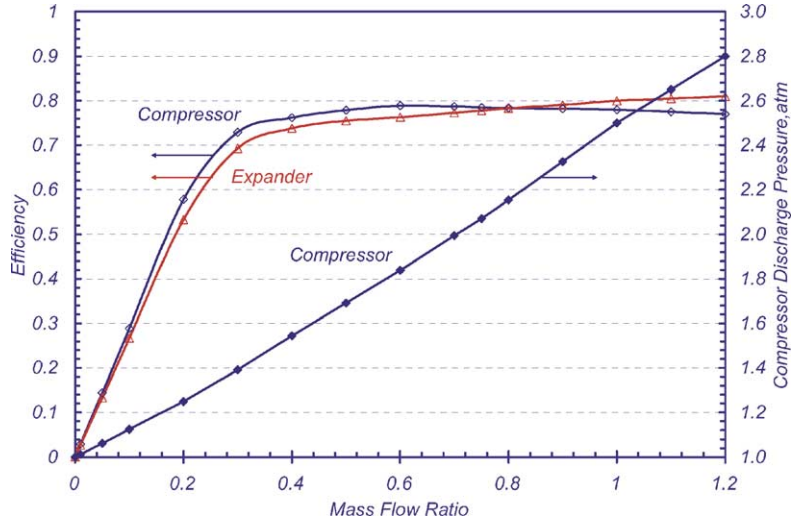

Fig. 5. CEM performance map: efficiencies and compressor discharge pressure.

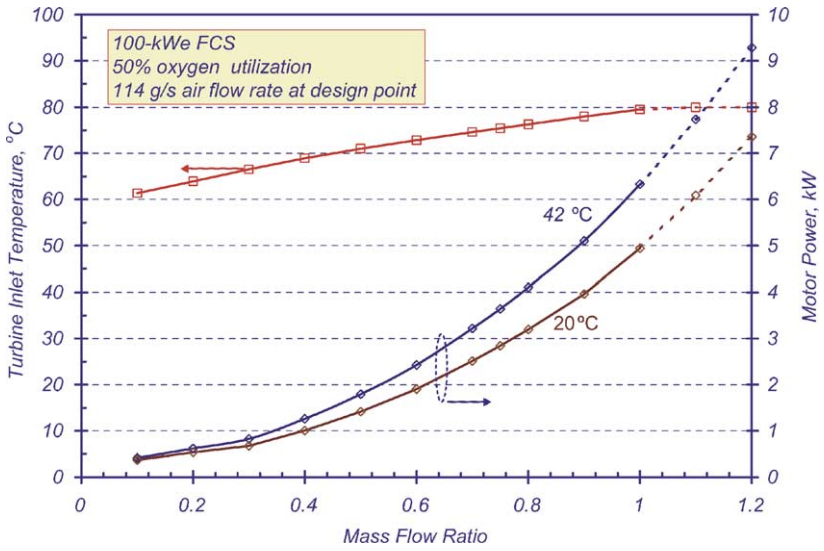

Fig. 6. Turbine inlet temperature and required motor power for 100 kWe FCS.

expander efficiencies drop off at part load. We estimate that the compressor can obtain a peak discharge pressure of 2.8 atm at 120% of the rated flow without compressor surge or choking in the nozzle. Under certain conditions, the peak pressure may be limited by the available motor power.

Fig. 6 shows the turbine inlet temperature which at steady state equals the dew point temperature to which the spent cathode air must be cooled in the condenser for process water recovery. Also shown is the calculated motor power needed to drive the CEM for the 100 kWe FCS. In calculating the shaft power we have allowed 3 psi (20.4 kPa) pressure drop between the compressor and expander at rated flow and have assumed that the pressure drop scales up linearly with flow. Fig. 6 indicates that at 42 °C ambient temperature 6.2 kW is needed at the shaft at rated flow. The system actually needs a motor larger than 6.2 kW to satisfy the requirement of 1 s response time. In our modeling analysis, we determined the motor size such that the air management system can adjust to provide the cathode flow necessary for the FCS power to increase from 10% to 90% of rated power in 1 s. Assuming that the motor can be overloaded by 50% for 1 s, we calculate that the 100 kWe FCS requires a motor of 9.3 kW rated power. With the oversized motor, the air management system can continuously supply 120% of the rated flow at 42 °C ambient temperature if the stack is warm (80 °C stack/turbine inlet temperatures) and 110% of the rated flow if the stack is cold (20 °C ambient and stack/turbine inlet temperatures). At 20 °C ambient temperature, the maximum capacity of the air management system is greater than 120% if the stack is warm (80 °C stack/turbine inlet temperatures).

Fig. 7 presents the modeled performance map of a 9.3 kW motor for the 100 kW FCS. It shows the steady-state power

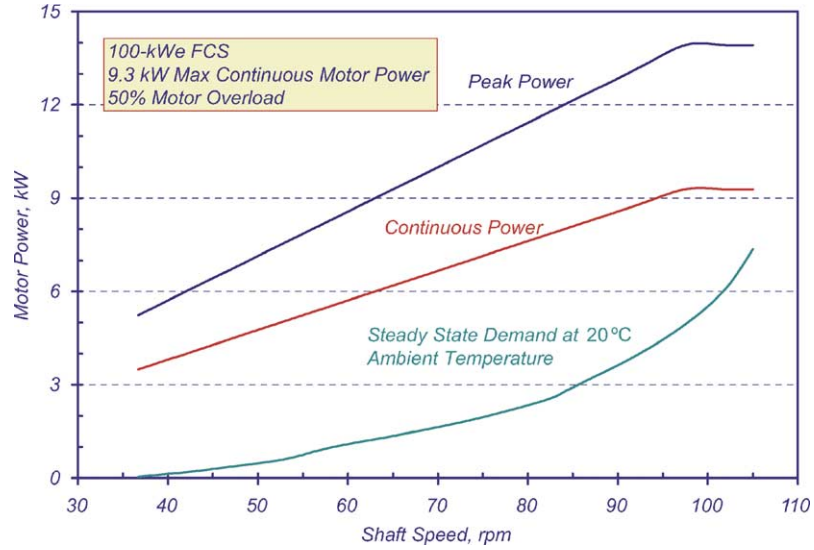

Fig. 7. Modeled performance map of a high-speed induction motor for 100 kWe FCS.

demand on the CEM shaft and the continuous power that the motor can provide as a function of the shaft speed. Also included in Fig. 7 is the peak power that the motor can develop under transient conditions assuming that the motor can be overloaded by 50% for up to 1 s.

A simulation was run to model the dynamic response of the CEM using the performance maps presented in Figs. 5 and 7 and assuming that the compressor, expander and motor are mounted on a common shaft and have a combined inertia of 2.5×10^{-4} kg m^2. The simulation showed that the modeled CEM can be accelerated from idle condition to rated flow in 1 s thus satisfying the target response time for 10–90% power. The calculated transient time is the minimum time since the motor was overloaded to the allowable limit during the entire simulation.

Maximum turndown of the turbo compressor–expander is an important parameter that affects the system efficiency at part load as well as oxygen utilization and water balance. It is determined by the minimum idle speed defined as the shaft rpm at which the air management system can provide sufficient cathode air to enable the FCS to generate the power needed by the CEM. In general, the idle speed may be determined by the power input to the motor controller and by the design of the CEM. For example, in the Honeywell design the air bearings require minimum rpm of 36,000 to support the shaft. Our simulations for the high-speed turbo compressor/expander indicate that with an expander in the system the idle speed can be as low as 42,500 rpm and the corresponding maximum turndown as high as 20. Without an expander, the idle speed can be as high as 51,500 rpm and the corresponding maximum turndown as low as 5.

3.3. Thermal and water management systems

Fig. 8 shows the heat duties of the humidifiers, traction inverter motor, condenser and radiators as function of vehicle speed for 65 and 120 kWe fuel cell systems. For the 120 kWe FCS, the heat duty of the high-temperature radiator is highest (about 32 kW) at the 100 mph top sustained speed, decreases as the vehicle speed is reduced, and is zero for vehicle speeds below 55 mph. There are several reasons why the radiator heat duty decreases with decrease in vehicle speed more steeply than the decrease in power demand with decrease in vehicle speed (see Fig. 3). One is that as the power demand goes down, the stack operating point moves up the polarization curve. Associated with the increase in cell voltage is higher efficiency and lower production of waste heat in the stack. A more important reason is related to the configuration of the FCS being considered. In this configuration, the high-temperature radiator rejects the heat that is picked up by the coolant in the stack minus the heat transferred from the coolant to the cathode air (also anode hydrogen) humidifier/pre-heater. As the power demand goes down, the cathode air circulation rate decreases so that the compressor discharge pressure is lower (see Fig. 5). We have assumed that the cathode air and anode hydrogen are always humidified to 90% RH at stack temperature. The lower the pressure the larger the amount of water needed (per unit flow rate of

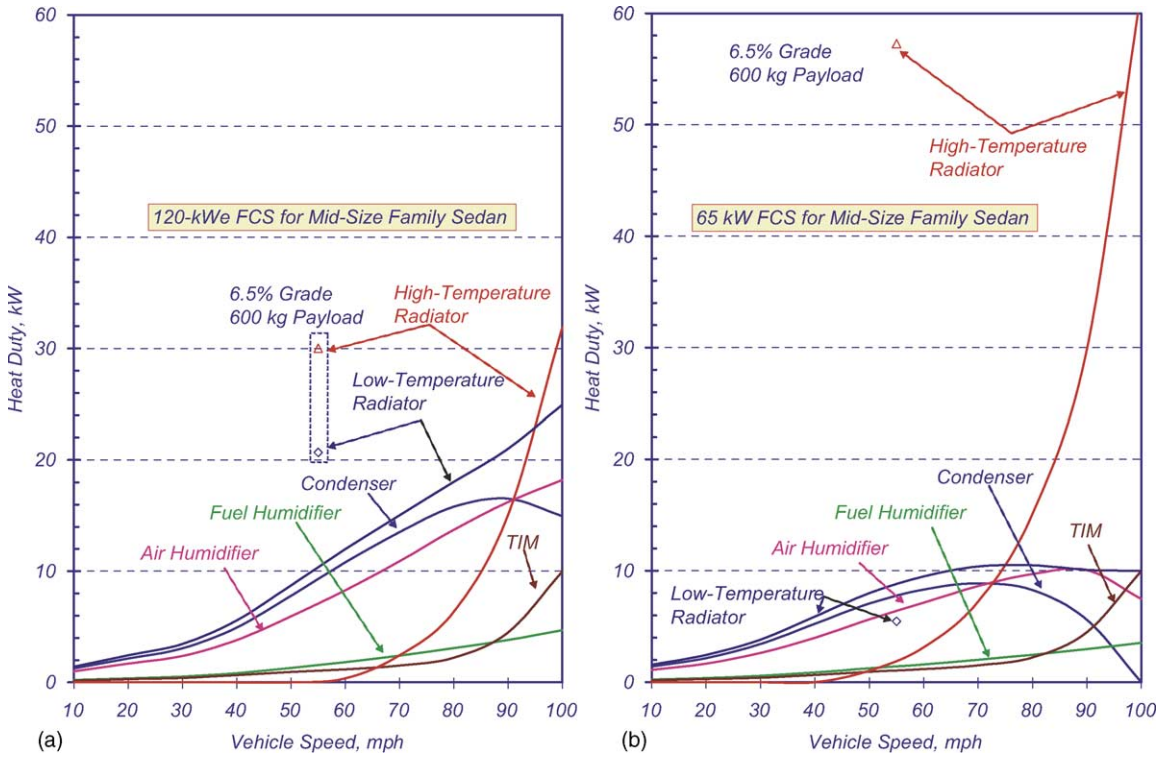

Fig. 8. Heat duties on FCS components and traction inverter motor: (a) 120 kWe FCS; (b) 65 kWe FCS.

air) to bring the cathode air to 90% RH and the higher the heat load in the humidifier. Results in Fig. 8a indicate that at vehicle speeds below 55 mph, all the waste heat picked up by the coolant in the stack is transferred to the cathode air and anode hydrogen across the humidifiers. An implication of zero heat rejection in the high-temperature radiator is that the stack cannot be maintained at its design temperature of 80 °C for prolonged driving below 55 mph.

The low-temperature radiator must reject the heat transferred to the coolant in the condenser and in the traction inverter motor. For the 120 kWe FCS, the condenser heat duty is 15 kW at 100 mph top sustained speed, increases as the vehicle speed is reduced until reaching a peak of about 17 kW at 85 mph, and decreases as the vehicle speed is reduced further. In the 100–85 mph range, the increase in condenser heat duty with reduction in vehicle speed is due to the lowering of the dew point temperature. At 100 mph, the traction power demand is 64 kWe, the system operates at 1.7 atm, and the dew point temperature to which the spent cathode air must be cooled in the condenser is 73 °C. At 85 mph, the traction power demand is 40 kWe, the system operates at 1.4 atm, and the dew point temperature is 69 °C. Thus, the increase in the condenser heat duty from 15 kW at 100 mph to 17 kW at 85 mph represents the additional cooling of the cathode air from 73 to 69 °C. In the 85–10 mph range, the decrease in condenser duty with reduction in vehicle speed results from the decreasing cathode air flow rate as the traction power demand goes down from 40 to 2 kWe which more than compensates for the lowering of the dew point temperature from 69 to 55 °C. The heat duty for the traction inverter motor increases monotonically with vehicle speed to reach 10 kW at 100 mph sustained top speed. The peak heat duty of the low-temperature radiator is 25 kW at the top speed and 21 kW at 6.5% grade.

Fig. 8b shows the heat duties of the various components for the 65 kWe FCS. Compared to the results for the 120 kWe FCS, the heat duties of the high-temperature radiator at 6.5% grade and at the top sustained speed are almost double even though the FCS is 50% smaller in rated power. At these driving conditions, the stack for the 65 kWe FCS operates at close to the rated power and system pressure (2.5 atm), and the system efficiency is 50%; the stack for the 120 kWe FCS, on the other hand, is at 50% of the rated power and 1.7 atm pressure, and the system efficiency is 55%. The combination of lower efficiency and higher pressure implies that the high-temperature coolant in the 65 kWe FCS absorbs more waste heat and latent heat of condensation in the stack for the 65 kWe FCS (72 kW) than in the stack for the 120 kWe FCS (55 kW). Also, heat duties of the air/fuel humidifiers/preheaters are lower in the 65 kWe FCS than in the 120 kWe FCS (12 kW versus 23 kW). Thus, at these driving conditions, the heat duty of the high-temperature radiator for the 65 kWe FCS is nearly twice that for the 120 kWe FCS (72 kW minus 12 kW versus 55 kW minus 23 kW).

Fig. 8 indicates that the peak heat duties of the low-temperature radiator (10 kW) and the condenser (8 kW) in the 65 kWe FCS are less than one-half of those in the 120 kWe FCS. In fact, the heat duty of the condenser for the 65 kWe FCS is zero at the top sustained speed (2.5 atm operating pressure) implying that the water added in the humidifiers condenses out in the stack itself. The peak heat duty of the condenser for the 65 kWe FCS occurs at lower vehicle speed (70 mph) than for the 120 kWe FCS (85 mph). In general, water management is easier in the 65 kWe FCS than in the 120 kWe FCS.

In fuel cell systems, the size of the radiator that rejects stack waste heat is of concern because the coolant temperature is limited to 80 °C. In order to address this concern, we have formulated and used simple heat transfer and fluid mechanics [8] models of ram air cooled radiators for a hybrid fuel cell propulsion system. In applying the model we assumed that the low-temperature radiator has the same frontal area (see Table 3) as the high-temperature radiator and is located directly in front of it since we prefer that the ambient air cool the low-temperature coolant first. We further assumed that a single-speed radiator fan supplies a pressure head of 380 Pa (2″ of water), and the coolant flow in the high-temperature circuit is proportional to the stack power and in the low-temperature circuit is proportional to the heat duty of the condenser and traction inverter motor.

A combinatorial method was used to determine the smallest size of the radiator that can satisfy the heat duty requirements under all driving conditions on the warmest day (taken as 42 °C in this study). It was found that a cross-flow radiator of plate-fin construction with 60 cm × 50 cm frontal area and 1 mm high coolant passages that are 9 mm apart can suffice. The fins on the air side of the radiator have 1 mm pitch. The depth of the flow passages was determined from the calculated heat transfer area to be 5.4 cm for the high-temperature radiator and 4.5 cm for the low-temperature radiator for a 120 kWe FCS. Fig. 9a presents the performance of the high-temperature radiator as a function of vehicle speed. It compares the required heat duty of the radiator and its maximum

Table 3
Radiators for FCS

FCS rated power	Radiator depth (cm)		Weight (kg)
	High temperature	Low temperature	
120 kW	5.4	4.5	21.9
65 kW	12	1.6	30.0

Frontal area	Pitch
60 cm × 50 cm	1.25 mm

Radiator fan	
Power	Head
700 W	380 Pa

Coolant inlet temperature	
HT radiator	LT radiator
70–80 °C	55–70 °C

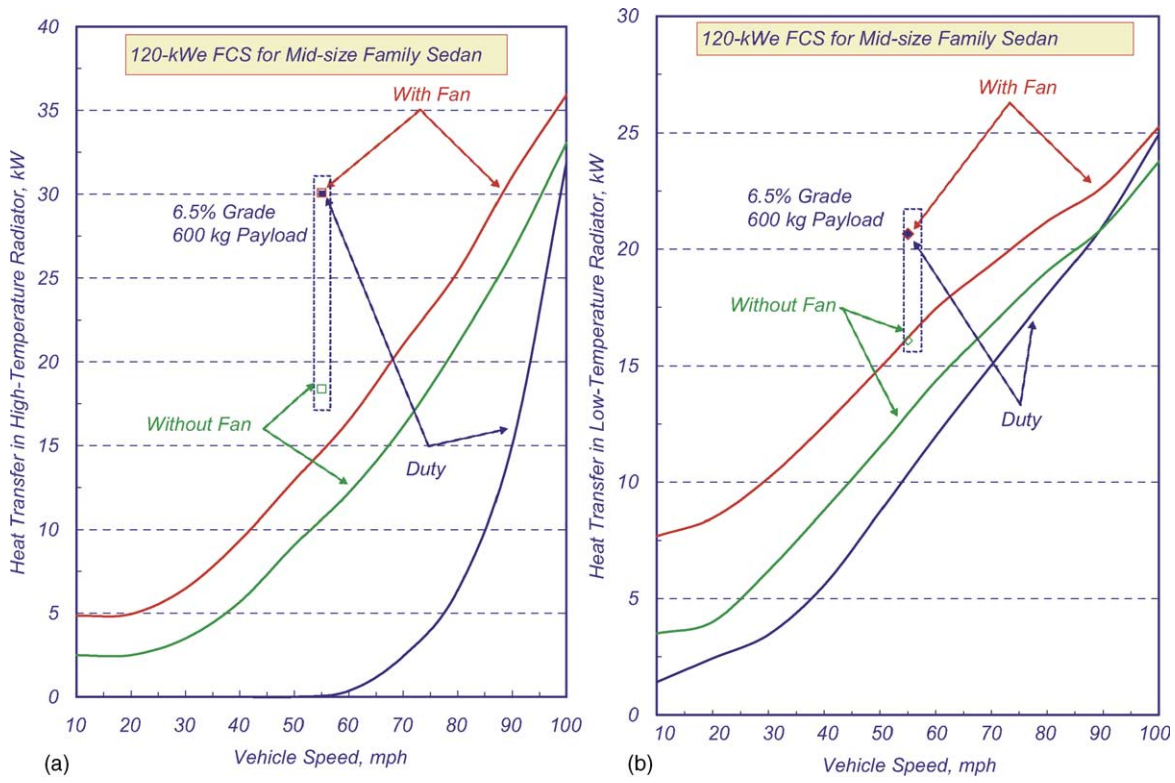

Fig. 9. Performance of high-temperature and low-temperature radiators for 120 kWe FCS: (a) high-temperature radiator; (b) low-temperature radiator.

heat rejection capability with and without the assistance of the blower fan. We estimate the heat rejection capability of the radiator by assuming that the coolant leaves the radiator at 70 °C and calculating the coolant inlet temperature from the coolant flow rate and the stack heat load. Because the estimated heat rejection capability without the blower fan exceeds the required heat duty, ram air alone can cool the radiator at all sustained speeds and a thermostatic control valve is needed to have a portion of the high-temperature coolant bypass the radiator. For sustained speeds below 55 mph, the coolant must bypass the radiator entirely. Fig. 9a also shows that the blower fan is needed to satisfy the heat duty requirement on 6.5% grade at 55 mph. The results in Fig. 9a imply that the depth of the flow passages is determined by the heat duty on 6.5% grade.

Fig. 9b compares the maximum heat rejection capability of the low-temperature radiator for the 120 kWe FCS (4.5 cm deep flow passages) with the heat duty imposed by the cooling requirements for the condenser and traction inverter motor. In determining the heat rejection capability we assume that the coolant enters the low-temperature radiator at 70 °C. Fig. 9b indicates that the blower fan is needed to satisfy the heat duty at 6.5% grade and for vehicle speeds above 90 mph.

Table 3 indicates that the high-temperature radiator for the 65 kWe FCS is larger in size than the one for the 120 kWe FCS although the low-temperature radiator is more compact. Compared to a radiator for a conventional ICE vehicle on the same platform [9], the frontal area of the radiators for the two fuel cell systems is about 40% larger and the surface area of the fins is much larger. Also, the grill has to be designed for >50% greater ram air which together with the larger fin area is likely to result in significant enhancement of the aerodynamic drag on the vehicle due to the FCS cooling system [8].

4. Performance of fuel cell systems for hybrid vehicles

Each of the four systems listed in Table 2 has the same efficiency at rated power (50%) and at 25% of the rated power (59.6%). At maximum continuous power (65 kWe), the 120 kWe FCS has the highest efficiency (57%) and the 65 kWe FCS the lowest efficiency (50%). The listed efficiencies are based on the net dc power produced by the FCS and lower heating value of hydrogen and account for all the parasitic losses (such as due to CEM, coolant pump and blower fan) within the fuel cell system.

Also included in Table 2 are the specific power of the fuel cell systems and the start-up times from cold. The listed specific powers account for the weights of the hydrogen storage media. It is assumed that hydrogen is stored as compressed gas at 5000 psi and in sufficient quantity for 320 mile driving range [1]. The estimates are based on assumed stack specific power of 800 W kg^{-1} at the rated power at 80 °C stack temperature.

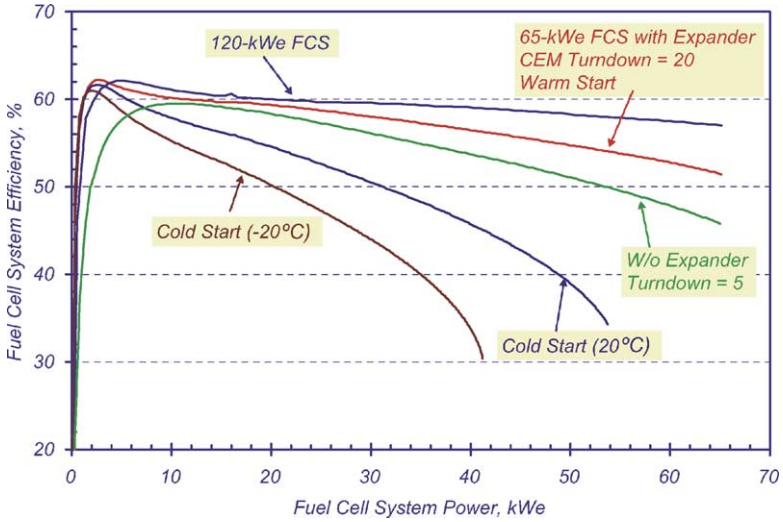

Fig. 10. FCS efficiency at constant load.

4.1. Efficiency at constant load

Fig. 10compares the efficiencies of the fuel cell systems of different power rating and under various conditions. The efficiencies plotted in this figure are at constant loads and prescribed stack temperatures. The assumption of constant load implies that no additional power is needed to accelerate the CEM shaft. The assumption of prescribed stack temperature implies that the plotted efficiencies are not steady-state values.

At 80 °C stack temperature, Fig. 10 indicates that the 65 kWe FCS has an efficiency of 50% at its rated power and that the efficiency increases as the load is reduced (because of increasing cell voltage) reaching a peak value of 61.5% at about 3 kWe. Further reduction in load below 3 kWe causes the efficiency to decrease primarily because of the turndown limitation of the CEM. In the low load region (<3 kWe), power consumed by the CEM is constant, and oxygen utilization is less than 50% and decreases as the load is reduced.

At 80 °C stack temperature, the 120 kWe FCS exhibits the same behavior as the 65 kWe FCS except that at a given load it has higher efficiency. The differences in efficiencies between the 65 and 120 kWe systems diminish as the load is reduced.

Also included in Fig. 10 is the efficiency of a 65 kWe FCS without an expander. At 80 °C stack temperature, it has 45% efficiency at rated power and a peak efficiency of about 59% at about 15 kWe load. Compared to the 65 kWe FCS with expander, its efficiency is smaller at rated power because of greater power consumption by the air management system; the efficiency is smaller at low loads because of the lower available turndown (20 with expander and 5 without expander).

Fig. 10 also shows the efficiency of 65 kWe FCS for cold start at 20 and −20 °C. At 20 °C stack temperature, the

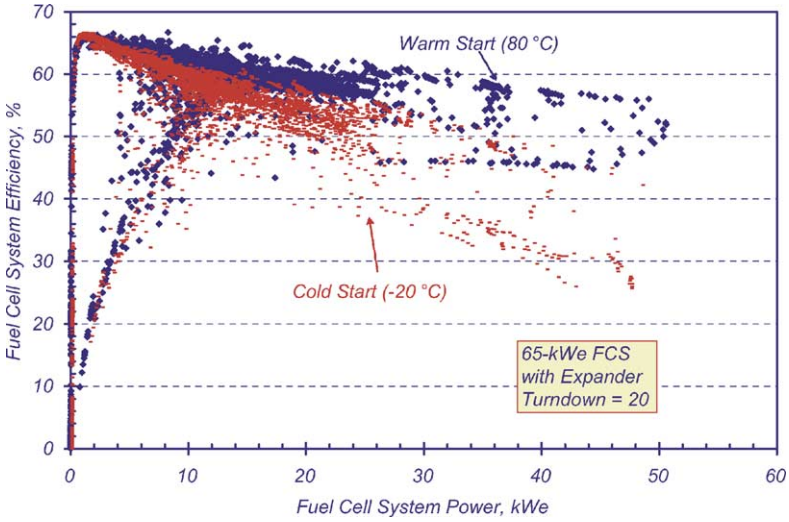

Fig. 11. Dynamic efficiency of FCS over simulated urban drive cycle.

maximum power that the FCS can generate with the oversized CEM is about 54 kWe. At this point, the cell voltage is 520 mV and the system efficiency is 34.5% compared to 55% at 80 °C stack temperature. At −20 °C ambient/0 °C stack temperature, the maximum power that the 65 kWe FCS can generate is further reduced to 41 kWe at which point the cell voltage is 450 mV and the system efficiency is 31% compared to about 58% at 80 °C stack temperature.

4.2. Dynamic efficiency

Fig. 11 is a scatter plot of the efficiency of the 65 kWe FCS for warm start on federal urban drive schedule (FUDS) [1]. The efficiency curve has two branches that are especially wide apart at low FCS power. The lower branch corresponds to FCS performance during periods of vehicle acceleration from zero or slow speeds with the CEM shaft spinning near its idle speed. In order to meet the sudden surge in power demand, our dynamic simulation model attempts to rapidly increase the cathode air flow rate by increasing the shaft speed. This requires the CEM motor/controller to draw large power from the PEFC stack degrading the efficiency of the FCS. During an acceleration event the dynamic efficiency of the FCS is lower than the steady-state efficiency at the same power. Conversely, the dynamic efficiency can be greater than the steady-state efficiency during the deceleration events because some of the CEM parasitic power can be supplied by the inertial power stored in shaft, compressor, expander and motor. The upper branch of the efficiency curve corresponds to FCS performance during periods of deceleration and constant power demand.

Deviations in FCS efficiency at constant power are also caused by dynamic variations in stack temperature and parasitic power consumed by the radiator fan. In our simulations the fan has single speed and is thermostatically controlled to maintain the stack in a narrow temperature range around 80 °C. The radiator fan is turned on when the stack temperature happens to exceed 80 °C + ΔT ($\Delta T \sim 2$ °C) and is turned off when it drops below 80 °C − ΔT. It is also turned on if the process water level in the tank falls below a set level.

Fig. 11 was constructed by including data every 1 s in the drive cycle simulation. The density of data points indicates that the power demand on FUDS is generally less than 30 kWe. As discussed earlier, the stack cannot be maintained at 80 °C if the sustained power is less than 12 kWe (cruising speeds below 50 mph). In our dynamic simulation the stack temperature was found to drop from 80 to 66 °C over the 1380 s long urban drive cycle. Over this cycle, the FCS has a cumulative efficiency of 59.2%.

Also included in Fig. 11 are the results from a simulation of the FCS performance on FUDS for cold start at −20 °C. As expected, the efficiency for cold start is lower than the efficiency for warm start and the differences in efficiency accentuate with FCS power. In our simulation, the PEFC stack was found to heat to about 22.5 °C at the end of the FUDS cycle.

For the urban drive cycle, Fig. 12 compares the dynamic efficiencies of two 65 kWe fuel cell systems: one with expander (FCS-1) and the other without expander (FCS-2). In these simulations, FCS-1 is assumed to have the maximum turndown achievable with an expander (20) and FCS-2 the maximum turndown achievable without an expander (5). The differences in efficiencies at high loads are due to the additional power generated by the expander. At low loads, where the parasitic power consumed by the CEM as a fraction of the power produced by the FCS is small, the differences in efficiencies are due to the larger turndown available with the expander. At low loads (10–20 kWe), FCS-1 shows a wide scatter in dynamic efficiency whereas FCS-2 exhibits minor fluctuations. At higher loads (20–50 kWe), efficiency fluctuations are damped in FCS-1 but are amplified in FCS-2. The amplitude of efficiency fluctuation is related to the CEM

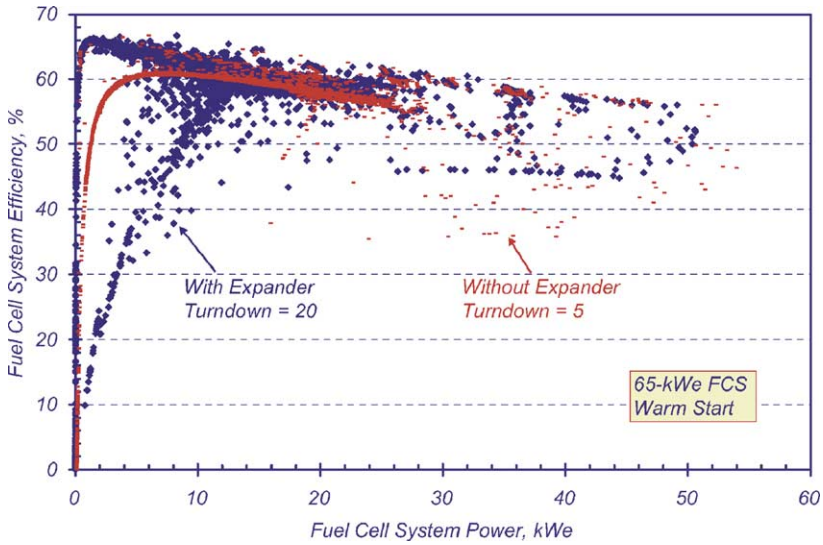

Fig. 12. Effect of expander on FCS dynamic efficiency.

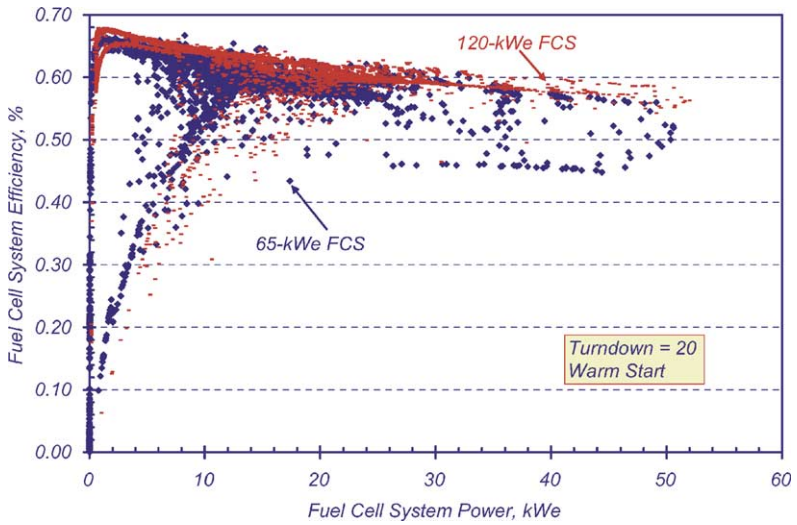

Fig. 13. Effect of FCS rated power on FCS dynamic efficiency.

motor power. The larger the motor power the higher the amplitude. FCS-2 has nearly three times larger motor power than FCS-1 and shows considerably greater scatter in efficiency.

Fig. 13 shows the effect of FCS rated power on dynamic efficiency for warm start on FUDS. At low power, the 120 kWe FCS displays a larger scatter in efficiency. On the other hand, the 65 kWe FCS exhibits larger scatter at high power. On FUDS, the 120 kWe FCS has a cumulative efficiency of 59.2% compared to 56.1% for the 65 kWe FCS.

4.3. System response times

Table 2 lists the transient response times of the fuel cell systems and the cold start-up times. The transient response time was determined by imposing a step change in power demand – from 10% to 90% of rated power – and calculating the time that the FCS takes to match the power demand. For the purpose of this calculation the initial temperature of the stack was assumed to be 80 °C and the ambient temperature was taken as 20 °C. The transient response time is primarily determined by the CEM that supplies air to the cathode. We selected the CEM motor which at 50% overload can increase the shaft speed from 47,000 to 92,200 rpm in 1 s. At 47,000 rpm the CEM provides cathode air needed by the FCS to produce 10% of rated power. At 92,200 rpm it provides cathode air needed by the FCS to produce 90% of rated power.

We similarly estimated the cold start-up times by imposing a step change in power demand – from 0% to 100% of rated power – and determining the time that the FCS takes to produce the rated power. For this calculation the initial stack temperature was assumed to be the same as the ambient temperature. Our simulations indicate that the stack must be above 45 °C in order for the FCS to produce the rated power. Thus, the cold start-up time essentially denotes the time required to heat the stack to 45 °C. The stack is heated primarily by the waste heat it generates. In our simulations we expedite the heat-up process by using the thermostatic valve to have the high-temperature coolant bypass the radiator. We estimate a start-up of time of 19.2 s from 20 °C ambient temperature and 34.4 s from −20 °C ambient/0 °C stack temperature.

5. Conclusions

In this paper, we have analyzed the design attributes and performance of load-following fuel cell systems for hybrid vehicles with an energy storage device that is operated in a charge-sustaining mode. The analysis has led to the following major conclusions:

- The minimum power rating of the fuel cell system for this type of hybrid vehicle is determined by the vehicle power demand under sustained driving conditions. For the mid-size family sedan analyzed in this work, the minimum rating is determined by the traction power at the top sustained speed rather than at 55 mph at 6.5% grade.
- The architecture of the drive train may dictate the minimum cell voltage at which the stack can be operated. The capacity of the air management system determines the minimum cell voltage that can be reached.
- A fuel cell system can generate more than its rated power. The maximum FCS power may be limited by the power electronics (i.e. the minimum voltage that a cell is allowed to operate at) or the by the capacity of the air management system.
- Under cold start conditions the PEFC stack power is derated. For the polarization curves used in this study, the stack power is derated by 20% at 20 °C and by 35% at −20 °C.

- The peak power of the electric motor in the CEM must be selected to satisfy the requirement of 1 s transient response time for 10–90% of rated FCS power.
- The radiator that rejects the waste heat produced in the stack must be designed for service at the most stringent driving condition on the warmest day. Our simulations indicate that for the mid-size family sedan analyzed in this work, the radiator design point is the heat duty requirement at 55 mph at 6.5% grade. Also, the radiator size for a hybrid vehicle increases as the FCS rated power is reduced.
- In principle the radiator can be cooled by ram air alone when the vehicle is cruising. A thermostatic control is needed with the coolant entirely bypassing the radiator at sustained speeds less than about 55 mph. For the FCS configuration analyzed in this paper the stack cannot be maintained at 80 °C if it is operated at low loads for an extended period of time.
- A condenser is needed to recover process water that is used to humidify the anode and cathode streams. Our simulations simulate that the condenser design point depends on the rating of the FCS and generally does not coincide with the condition that imposes maximum heat duty on the radiator.
- Compared to a radiator for an internal combustion engine for the same vehicle platform, the high-temperature and low-temperature radiators for the FCS require larger frontal area, more ram air, larger blower fan and larger surface area of the fins. The FCS cooling air is likely to significantly enhance the aerodynamic drag on fuel cell vehicle.
- The dynamic efficiency of the FCS depends on many factors including the load, stack temperature, power rating of the FCS, and maximum CEM turndown. For specified load and stack temperature, there can be a wide scatter in system efficiency due to rapid variations in power demand caused by vehicle acceleration and deceleration. The scatter in efficiency is especially large when the CEM shaft is spinning close to the idling speed.

Acknowledgements

This work was supported by the U.S. Department of Energy's Office of Energy Efficiency and Renewable Energy, Office of Hydrogen, Fuel Cells, and Infrastructure Technologies and the Office of FreedomCAR and Vehicle Technologies.

References

[1] R.K. Ahluwalia, X. Wang, A. Rousseau, R. Kumar, Fuel economy of hydrogen fuel cell vehicles, J. Power Sources 130 (2004) 192–201.
[2] M.A. Weiss, J.B. Haywood, A. Schafer, V.K. Natarajan, Comparative Assessment of Fuel Cell Cars, Publication No. LFEE 2003-001 RP, Massachusetts Institute of Technology, Laboratory for Energy and the Environment, February 2003.
[3] Well-to-Wheel Energy Use and Greenhouse Gas Emissions of Advanced Fuel/Vehicle Systems – North American Analysis, vol. 2, General Motors Corporation, June 2001.
[4] H.K. Geyer, R.K. Ahluwalia, GCtool for Fuel Cell Systems Design and Analysis: User Documentation, Argonne National Laboratory Report, ANL-98/8, 1998.
[5] GM/Opel Set First Fuel Cell Records with HydroGen1, Releases New Stack Design Details, Hydrogen and Fuel Cell Letter, ISSN: 1080-8019, June 2001.
[6] Ballard Sets New Standards for Automotive Fuel Cells, News Release, October 26, 2001, www.ballard.com.
[7] M.K. Gee, Fuel Cell Turbocompressor, DOE Hydrogen, Fuel Cells and Infrastructure Technologies Program 2003 Merit Review and Peer Evaluation Meeting, Berkeley, CA, May 19–22, 2003.
[8] R.H. Barnard, Theoretical and experimental investigation of the aerodynamic drag due to automotive cooling systems, in: Proceedings on Institution of Mechanical Engineers, vol. 214, Part D, 2000, pp. 919–927.
[9] J.B. Heywood, Internal Combustion Engine Fundamentals, McGraw-Hill, New York, 1988.